International Journal of
*Molecular Sciences*

MDPI

*Article*

# Clusterin Promotes the Migration and Invasion of Highly Aggressive Breast Cancer Cells Through Molecular Mechanisms That Affect the Cell Cytoskeleton and Extracellular Matrix Dynamics

**Alessia Ciringione [1], Marina Marozzi [1], Silvana Belletti [2], Margot Lo Pinto [3], Simone Dario Scilabra [3], Patrizia Cancemi [4] and Federica Rizzi [1,5,6,*]**

1 Laboratory of Biochemistry, Molecular Biology and Oncometabolism, Department of Medicine and Surgery, University of Parma, Via Volturno 39, 43125 Parma, Italy; alessia.ciringione@unipr.it (A.C.); marinamarozzi91@gmail.com (M.M.)
2 Histology and Embryology Laboratory, Department of Medicine and Surgery, University of Parma, Via Volturno 39, 43126 Parma, Italy; silvana.belletti@unipr.it
3 Proteomics Group of Ri.MED Foundation, Research Department, IRCCS ISMETT (Istituto Mediterraneo per i Trapianti e Terapie ad Alta Specializzazione), Via E. Tricomi 5, 90127 Palermo, Italy; mlopinto@fondazionerimed.com (M.L.P.); sdscilabra@fondazionerimed.com (S.D.S.)
4 Department of Biological, Chemical and Pharmaceutical Sciences and Technologies (STEBICEF), University of Palermo, Viale Delle Scienze, Ed. 16, 90128 Palermo, Italy; patrizia.cancemi@unipa.it
5 National Institute of Biostructure and Biosystems (INBB), 00136 Rome, Italy
6 COMT-Center for Molecular and Translational Oncology, 43124 Parma, Italy
* Correspondence: federica.rizzi@unipr.it

## Abstract

Metastatic breast cancer (BC) remains a major clinical challenge, and identifying molecular mechanisms driving tumor cell migration and invasion is critical to develop effective therapeutic strategies. Clusterin (CLU), a secreted chaperone-like protein, is upregulated in BC and metastatic tissue; however, its functional contribution to tumor aggressiveness remains unclear. Here, we silenced CLU by siRNA in two BC cell lines with distinct aggressiveness and examined its impact on migration, invasion, and associated signaling pathways. Following CLU silencing, cell migration and invasion were assessed using transwell assays. Cytoskeletal organization was evaluated by F-actin staining, while downstream signaling pathways were analyzed by RT-PCR, Western blotting, and Rho GTPase pull-down. A comparative proteomic analysis was performed in CLU-expressing and CLU-silenced MDA-MB-231 cells. CLU knockdown significantly reduced migration and invasion in MDA-MB-231, concomitantly with loss of F-actin-rich membrane protrusions, reduced expression of MMP9, COL1A1, and COL4A1, and decreased activation of Akt, NF-κB, and RhoA. Proteomic profiling revealed extensive remodeling of pathways involved in cell adhesion, cytoskeletal dynamics, and extracellular matrix interactions. Differently, no or very mild effects were observed in CLU-silenced MCF-7 cells. These findings identify CLU as an upstream regulator of a pro-metastatic adhesion–cytoskeleton signaling in BC, selectively operative in EMT-engaged, basal-like cells, highlighting the importance of patient stratification for CLU-targeted therapeutic strategies.

**Keywords:** metastatic breast cancer; clusterin; CLU; cell migration; cell invasion; cell cytoskeleton; extracellular matrix

Check for updates

Academic Editor: Ioannis Boutas

Received: 14 January 2026
Revised: 4 February 2026
Accepted: 8 February 2026
Published: 10 February 2026

**Copyright:** © 2026 by the authors. Licensee MDPI, Basel, Switzerland. This article is an open access article distributed under the terms and conditions of the Creative Commons Attribution (CC BY) license.

## 1. Introduction

Breast cancer (BC) is the most frequently diagnosed cancer and the leading cause of cancer-related deaths in women worldwide [1]. Breast tumors are extremely heterogeneous, showing different morphological and biological characteristics and, consequently, variable clinical behaviors. One of the most used classifications in clinical practice is based on the differential expression of three cell surface receptors—the estrogen (ER), the progesterone (PR), and the human epidermal growth factor (HER2) receptors—identifying four subtypes of breast tumors: Luminal A, Luminal B, HER2-enriched and basal-like. The Luminal A subtype is ER- and PR-positive; it usually responds well to hormone blocker therapy and is the one with the best outlook among the molecular breast cancer subtypes [2]. The basal-like subgroup, also referred to as triple-negative breast cancer (TNBC), accounts for 15% of all breast cancer cases. It is characterized by low or no expression of *ER*, *PR*, and *HER2*; therefore, it does not respond to hormone therapy or anti-HER2 drugs, presents an aggressive clinical behavior, and bears the worst prognosis [3,4]. Since an invasive phenotype is among the main causes of high mortality in BC patients, investigating the molecular mechanisms that favor BC metastasis is essential and may help to identify new druggable targets to block the escape of cancer cells from the primary site.

Clusterin (CLU), first discovered and isolated from ram rete testis, is a secreted heterodimeric glycoprotein of approximately 76–80 kDa molecular mass, depending on the glycosylation degree, found in almost all human biological fluids and tissues [5]. *CLU* expression is upregulated following many different stimuli, including heat shock, hypoxia, ionizing radiation, and chemotherapeutics, and more generally under stressing and pro-inflammatory conditions [6]. Transcriptional, translational, and post-translational mechanisms contribute to the fine-tuning of *CLU* expression, including tissue-specific epigenetic mechanisms that involve DNA methylation and histone post-translational modification [7]. CLU plays a central role in diverse cellular processes, such as cell death, inflammation, and tissue remodeling, possibly because of its chaperone-like function [8].

Despite the great amount of literature on CLU expression and action in different tumor types, its role in cancer progression and metastasis remains controversial [9–12]. Indeed, CLU primarily acts as a tumor suppressor in the early stages of carcinogenesis [13–15]; conversely, high levels of CLU may provide a pro-survival stimulus by enhancing resistance to anti-cancer therapies and tumor cell survival in specific microenvironmental niches [16]. In BC, high levels of CLU have been found in malignant lesions compared to normal tissue [17], although its prognostic and predictive value during progression is unclear [18]. For instance, while combined treatments using anti-CLU antibodies or oligonucleotides with paclitaxel or other chemotherapeutic drugs have shown additive cytotoxic effects in vitro and in vivo [16,19], a phase II clinical trial evaluating OGX-011, a second-generation antisense oligonucleotide, in combination with docetaxel, did not yield any additive effect compared to single-agent treatment [20]. Thus, elucidating the biological role of CLU in sustaining BC aggressiveness is crucial to bridge the gap between encouraging preclinical results and successful clinical translation.

The present work aimed to study the effects of CLU knockdown in MCF-7 and MDA-MB-231, two cancer cell lines widely used to mimic progressive stages of BC aggressiveness. The MCF-7 molecular profile resembles many characteristics of the Luminal A subtype, while the molecular features of the MDA-MB-231 cell line share many similarities with basal-like TNBC. We focused our investigation on proliferation, migration, invasion, epithelial–mesenchymal transition (EMT), and intracellular signaling pathways involved in extracellular matrix (ECM) remodeling and cytoskeletal fiber dynamics. Moreover, we performed a proteomic analysis to identify downstream molecular effectors of CLU knockdown and related signaling pathways.

## 2. Results

### *2.1. CLU Silencing Does Not Affect the Cell Viability of BC Cell Lines*

Firstly, we assessed the basal expression levels of CLU in both BC cell lines by Western blot analysis. CLU appeared as two distinct bands: one with a molecular weight of approximately 60 kDa, corresponding to the uncleaved partially glycosylated precursor protein (pCLU), and one with a molecular weight of about 40 kDa, corresponding to the mature α and β chains of the mature protein ready for secretion (sCLU). MCF-7 cells showed higher basal levels of sCLU compared to MDA-MB-231 cells (Figure 1a).

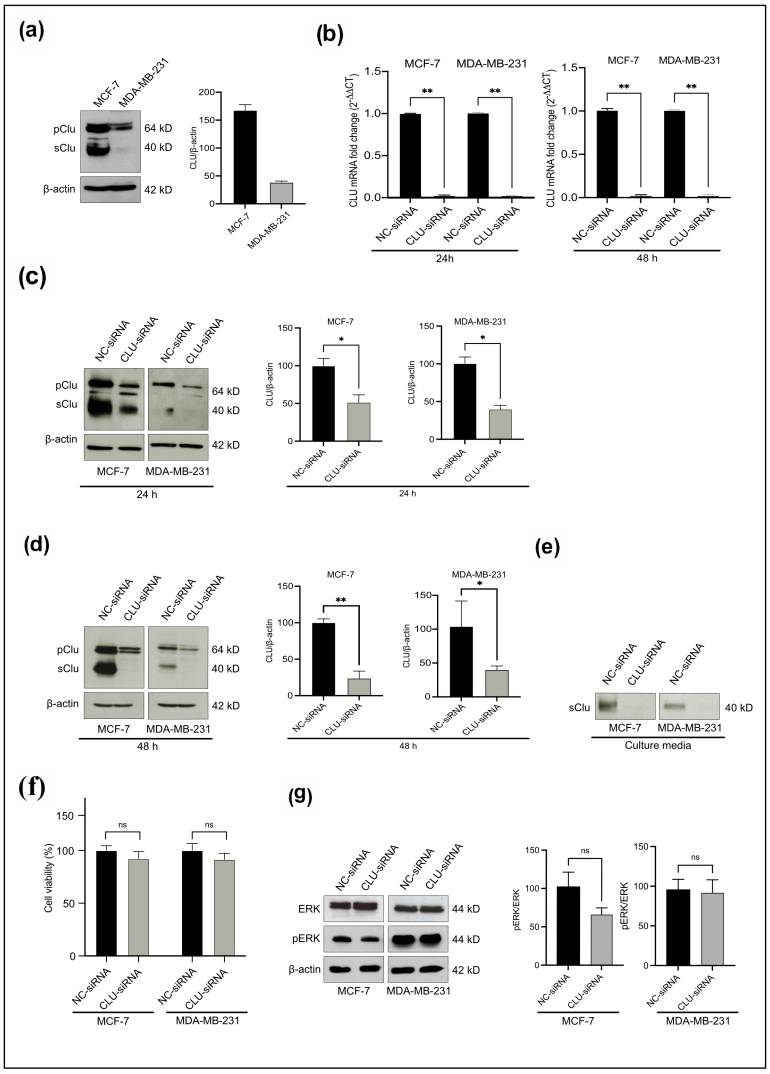



**Figure 1. CLU silencing does not affect cell viability in MCF-7 and MDA-MB-231 cell lines**. Basal expression of CLU in MCF-7 and MDA-MB-231 cell lines assessed by Western blot. Densitometric analysis reports the expression of CLU normalized to β-actin levels. pCLU = CLU precursor; sCLU = secreted CLU (**a**). CLU mRNA levels at 24 and 48 h after transfection with CLU-siRNA or NC-siRNA were assessed by q-RT-PCR. The mRNA fold change of CLU mRNA measured in CLU-siRNA cells compared to NC-siRNA was calculated by the $2^{-\Delta\Delta CT}$ method (**b**). Western blots of cell lysates at 24 h and 48 h post-transfection (**c**,**d**). CLU levels in conditioned media (**e**). Cell viability measured with a luminescence assay 48 h after transfection. The bar graph shows the % of cell viability of CLU-siRNA cells compared to NC-siRNA cells (**f**). Expression of phosphorylated ERK (pERK) assessed by Western blot. The densitometric analysis shows the fold change of pERK/ERK ratios in CLU-siRNA compared to NC-siRNA, normalized for β-actin levels (**g**). Error bars represent the SD of the mean of three independent experiments. Statistical significance was determined by Student's *t*-test (ns = non-significant; * $p \leq 0.05$; ** $p \leq 0.01$).

Subsequently, we transfected both MCF-7 and MDA-MB-231 cells with either CLU-specific siRNA (CLU-siRNA) or negative control siRNA (NC-siRNA). A significant reduction in CLU mRNA levels (over 90%) (Figure 1b) was achieved in both cell lines 24 h after CLU-siRNA transfection, compared to NC-siRNA. The reduction was maintained up to 48 h. In MCF-7 cells, CLU protein levels were reduced by 42% and 75% at 24 and 48 h after transfection, respectively, compared to controls (Figure 1c,d). In MDA-MB-231 cells, CLU protein levels were reduced by 61% at both 24 and 48 h after transfection compared to controls (Figure 1c,d). Of note, sCLU expression was undetectable in the culture media of both cell lines 48 h after silencing (Figure 1e). Despite the significant reduction in CLU expression, silencing did not significantly affect cell viability in either MCF-7 or MDA-MB-231 cells (Figure 1f). Consistently, no differences were observed in the expression of the phosphorylated ERK (pERK) in either cell line (Figure 1g).

### *2.2. CLU Knockdown Reduces the Migration and Invasion of MDA-MB-231 Cells but Has No Significant Effects on MCF-7 Cells*

To investigate whether CLU regulates BC cell motility, we first performed transwell migration assays in MCF-7 and MDA-MB-231 cells transfected with CLU-siRNA or NC-siRNA (Figure 2a). CLU silencing did not significantly affect the migratory behavior of MCF-7 cells. In contrast, CLU knockdown significantly reduced migration in MDA-MB-231 cells by approximately 21% compared to controls. To further assess the specificity of CLU involvement in BC cell migration, rescue experiments were conducted by treating CLU-silenced MDA-MB-231 cells with recombinant CLU protein. As expected, recombinant CLU significantly restored the migratory capacity of CLU-depleted cells, supporting a direct role of CLU in regulating BC cell migration (Figure S1).

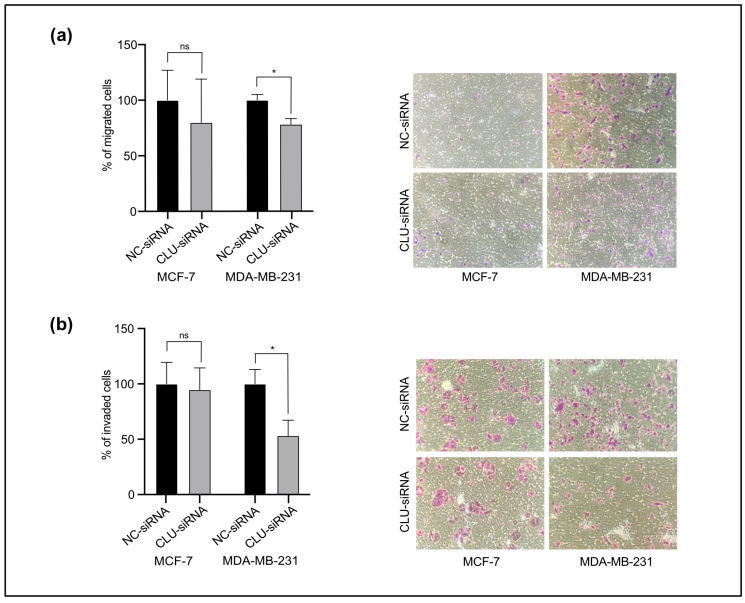



**Figure 2. Effects of CLU knockdown on cell migration and invasion in MCF-7 and MDA-MB-231 cell lines**. Transwell migration (**a**) and invasion (**b**) assays of MCF-7 and MDA-MB-231 cell lines transfected with CLU-siRNA or NC-siRNA. Cells that migrated through an uncoated insert (migration) or a Matrigel-coated insert (invasion) were fixed, crystal violet-stained, and counted under a light microscope at 200X magnification. The bar graphs show the ratio of CLU-siRNA cells/NC-siRNA cells x100. Data represent mean ± SD from three independent experiments. Statistical significance was determined by the Student's *t*-test (ns = non-significant; * $p \leq 0.05$).

We then evaluated the impact of CLU depletion on invasive behavior using transwell invasion assays (Figure 2b). While invasion was unaffected in MCF-7 cells, CLU knockdown

resulted in a significant reduction in invasion (approximately 50%) in MDA-MB-231 cells compared to controls. To account for differences in baseline migration, we calculated an invasion index (invaded/migrated cells) for each biological replicate. Normalization confirmed that CLU knockdown significantly reduced the invasion index in MDA-MB-231 cells, indicating that CLU depletion specifically impairs invasive capacity beyond its effect on migration (Figure S2).

### *2.3. CLU Does Not Affect the Expression of EMT Markers in BC Cells*

Epithelial-to-mesenchymal transition (EMT) encompasses progressive changes in cellular organization from an epithelial to a mesenchymal phenotype, favoring cancer cell migration and invasion [21]. To investigate whether CLU expression influences EMT, we evaluated EMT-inducing transcription factors and canonical EMT markers in both BC cell lines. CLU silencing significantly reduced Slug expression in both cell lines, whereas Snail expression was selectively upregulated in MCF-7 cells (Figure 3a). As expected, MDA-MB-231 cells expressed high levels of Vimentin and lacked E-cadherin expression, while MCF-7 cells showed the opposite pattern (Figure 3b,c). CLU silencing did not affect E-cadherin or Vimentin expression in either cell line (Figure 3b,c). Immunocytochemistry confirmed that CLU silencing did not impact E-cadherin or Vimentin localization (Figure 3d), indicating that CLU can selectively modulate EMT-related transcription factors without altering the underlying epithelial or mesenchymal phenotype.

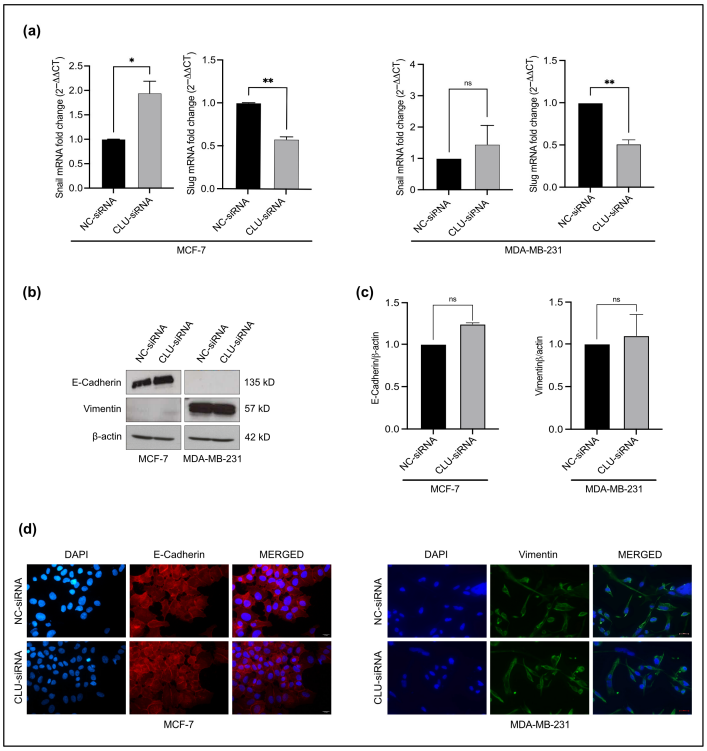



**Figure 3. Effects of CLU knockdown on EMT**. Relative mRNA levels of Snail and Slug were measured by qRT-PCR in MCF-7 and MDA-MB-231 cells transfected with CLU-siRNA or NC-siRNA. The mRNA fold change of each mRNA in CLU-siRNA cells compared to controls was calculated by the $2^{-\Delta\Delta CT}$ method (**a**). Protein expression levels of E-cadherin and Vimentin were measured by Western blot (**b**), and densitometric analysis is shown as fold change of E-cadherin and Vimentin expression in CLU-siRNA cells compared to NC-siRNA cells, normalized to β-actin (**c**). Data represent mean ± SD of three independent experiments. Statistical significance was determined by the Student's *t*-test (ns = non-significant; * $p \leq 0.05$; ** $p \leq 0.01$). Immunocytochemistry of E-cadherin (red fluorescence) and Vimentin (green fluorescence) in MCF-7 and MDA-MB-231 cells transfected with CLU-siRNA or NC-siRNA (**d**). Nuclei were counterstained with DAPI (blue fluorescence). Scale bar = 20 μm.

### *2.4. CLU Knockdown Induces Modification of the Cytoskeleton of MDA-MB-231 Cells*

Actin and tubulin, two key protein components of the cytoskeleton, play crucial roles in maintaining cell shape and motility [22]. Since cytoskeletal remodeling is tightly linked to cell migration properties [23], we evaluated the effects of CLU silencing on the actin–tubulin network by confocal laser scanning microscopy (CLSM) analysis. Phalloidin staining showed that control MDA-MB-231 cells exhibited actin organized into well-defined fibers, several F-actin-rich membrane protrusions, ruffles, and thick stress fiber bundles across the cell surface (Figure 4b). Microtubules displayed a dense, evenly distributed network (Figure 4d). Upon CLU silencing, MDA-MB-231 cells appeared more elongated with a less structured acto-tubulin network (Figure 4b–d). In addition, a marked reduction in F-actin-rich membrane protrusions, ruffles, and stress fibers were detected (Figure 4b), as well as a reorganization of microtubules into oriented bundles along the major axis (Figure 4d). MCF-7 cells maintained their cobblestone-like epithelial morphology, with few protrusions or stress fibers, and showed no detectable cytoskeletal changes upon CLU knockdown (Figure 4a–c).

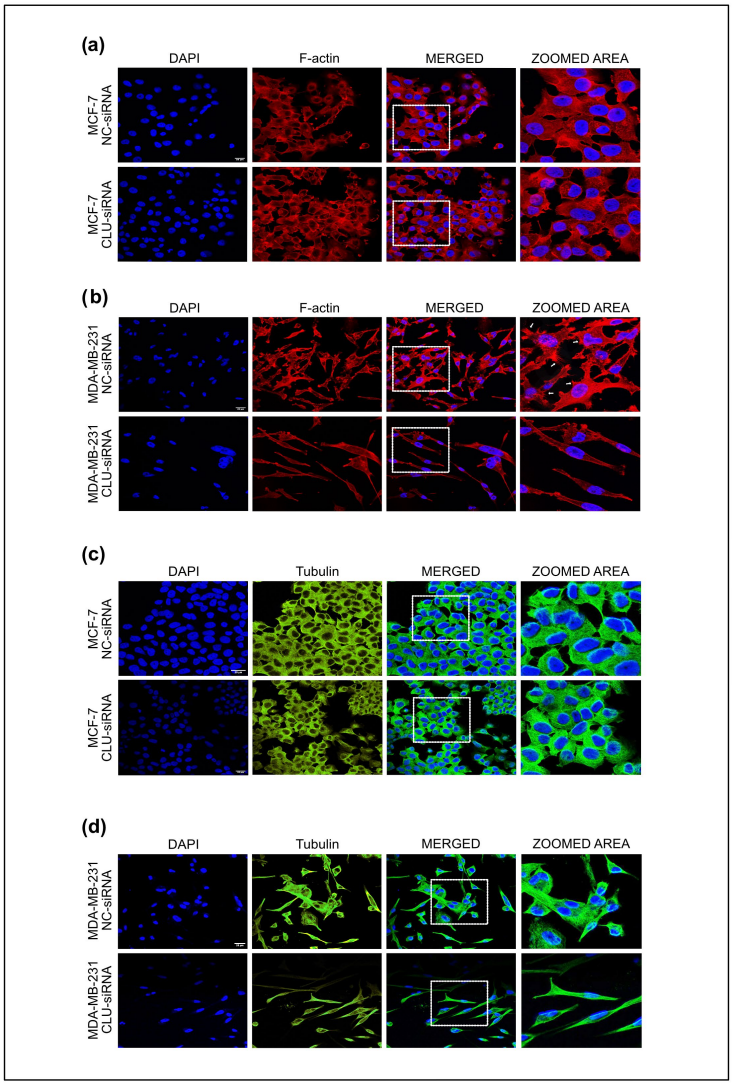



**Figure 4. Effects of CLU silencing on the cytoskeleton**. Phalloidin staining of actin filaments (red fluorescence) (**a**,**b**), and immunocytochemistry analysis of α-tubulin (green fluorescence) (**c**,**d**) in MCF-7 and MDA-MB-231 cells transfected with CLU-siRNA or NC-siRNA. White arrows indicate F-actin-rich membrane protrusions. Nuclei were counterstained with DAPI (blue fluorescence). Scale bar = 20 µm. Insets show digitally zoomed areas.

### *2.5. In MDA-MB-231 Cells, CLU Promotes Cell Motility by Acting on RhoA and Sustains Cell Invasion Through ECM Remodeling*

The small GTPase RhoA regulates actin polymerization during cell protrusion formation [24]. To assess whether CLU influences the intracellular signaling pathways involved in cytoskeletal dynamics, we first assessed RhoA activity using a pull-down assay. CLU silencing markedly reduced GTP-bound (active) RhoA in MDA-MB-231 cells, whereas no changes were observed in MCF-7 cells (Figure 5a). Consistent with impaired RhoA signaling, we observed reduced phosphorylation of Akt in CLU-silenced MDA-MB-231 cells (Figure 5b). A similar reduction was detected for phosphorylated NF-κB (Figure 5b), which led us to investigate downstream ECM-remodeling genes.

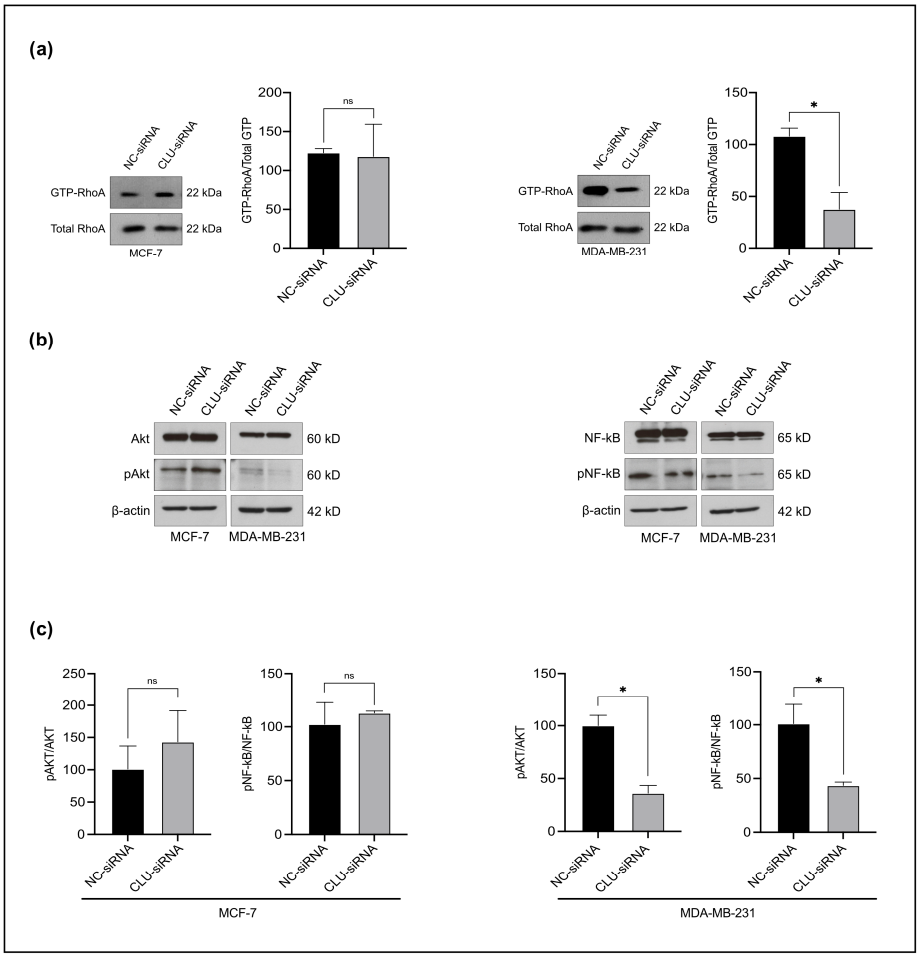



**Figure 5. Effects of CLU silencing on intracellular signaling pathways that control cell motility and invasion.** Following RhoA-GTP pull-down, the expression of RhoA-GTP in MCF-7 and MDA-MB-231 cells transfected with CLU-siRNA or NC-siRNA was measured by Western blot. The densitometric analysis shows the fold change of RhoA-GTP expression in CLU-siRNA compared to NC-siRNA, normalized for total RhoA levels (**a**). The expression levels of the phosphorylated (active) forms of Akt (pAkt) and NF-kB (pNF-kB) in MCF-7 and MDA- MB-231 cells transfected with CLU-siRNA or NC-siRNA were measured by Western blot (**b**). The densitometric analysis shows the fold change of pAkt/Akt and pNF-kB/NF-kB ratios in CLU-siRNA compared to NC-siRNA, normalized for β-actin levels (**c**). All the bar graphs show the mean ± SD of three independent experiments. Statistical significance was determined by the Student's *t*-test (ns = non-significant; * $p \leq 0.05$).

CLU silencing significantly decreased MMP9, COL1A1, and COL4A1 mRNA levels in MDA-MB-231 cells. In MCF-7 cells, MMP9 and COL1A1 remained unchanged upon CLU silencing, whereas COL4A1 was not detectable (Figure 6a,b).

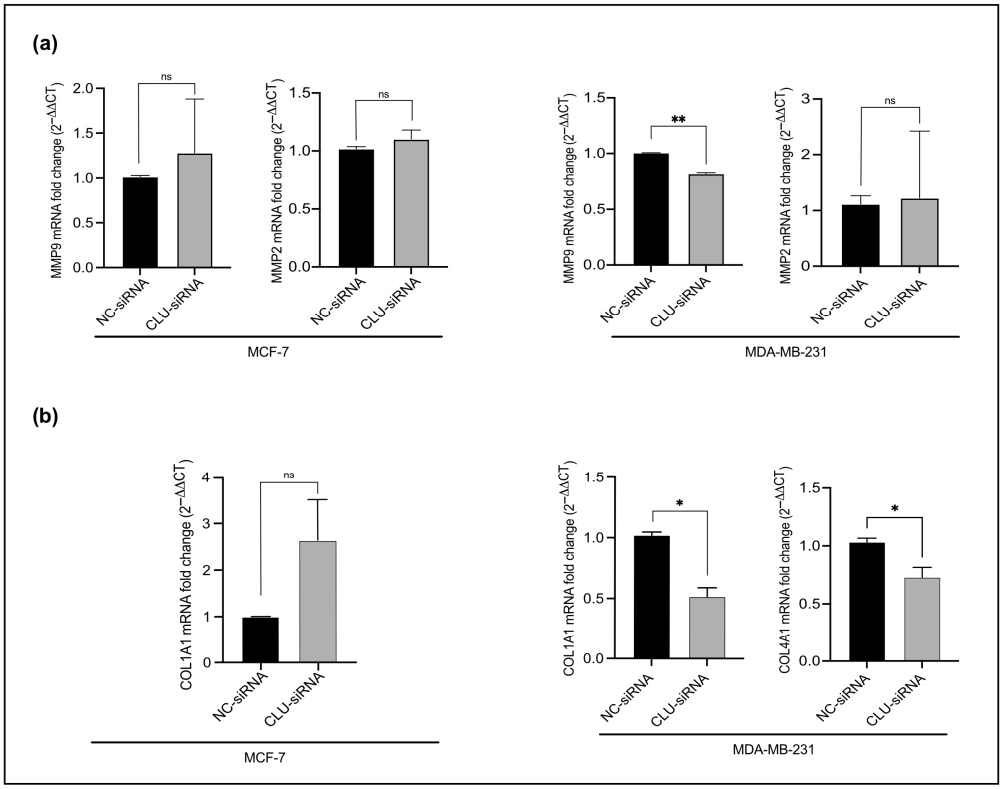



**Figure 6. Effects of CLU silencing on the expression of ECM-related genes**. The expression of MMP9, MMP2, COL1A1, and COL4A1 in MCF-7 and MDA-MB-231 cells transfected with CLU-siRNA or NC-siRNA was measured by qRT-PCR. The mRNA fold change in CLU-siRNA cells compared to controls was calculated by the $2^{-\Delta\Delta CT}$ method (**a**,**b**). All the bar graphs show the mean ± SD of three independent experiments. Statistical significance was determined by Student's *t*-test (ns = non-significant; * $p \leq 0.05$; ** $p \leq 0.01$).

### *2.6. CLU Knockdown Induces Proteomic Changes in MDA-MB-231 Cells*

To investigate the global proteomic changes induced by CLU knockdown, we performed a comparative proteomic analysis on proteins extracted from MDA-MB-231 cells transfected with either CLU-siRNA or NC-siRNA. Proteins were analyzed by high-resolution mass spectrometry using a data-independent acquisition (DIA) workflow for label-free quantification, enabling the identification of differentially abundant proteins between the two conditions. A total of 1197 proteins were identified (Table S1). After applying false discovery rate (FDR) correction for multiple testing, eleven proteins remained significantly altered upon CLU silencing. Among these, four proteins were upregulated (TLN1, NDRG1, ATP1B1, and PNPH), whereas seven proteins were downregulated (CCN1, UGDH, HEXIM1, AGR2, SLC38A2, SFXN3, and ENY2). These proteins represent the statistically robust, FDR-controlled proteomic changes associated with CLU depletion.

To place these FDR-significant changes into a broader biological context, we additionally performed exploratory pathway- and network-level analyses using a larger set of proteins showing differential abundance at a nominal *p*-value < 0.05 (corresponding to $-\log10(p\text{-value}) = 1.3$, dashed line in Figure 7a). Using this exploratory threshold, 135 proteins were differentially abundant, with 60 proteins increased and 75 decreased in CLU-siRNA cells compared to NC-siRNA controls. Functional relationships among these nominally significant proteins were analyzed using the STRING database (version 12.0). Protein–protein interaction (PPI) networks generated separately for up- and downregulated proteins showed significant enrichment ($p < 1.0 \times 10^{-16}$ and $p = 6.34 \times 10^{-8}$, respectively), indicating interaction rates higher than expected for random protein sets of similar size (Figure 7b).

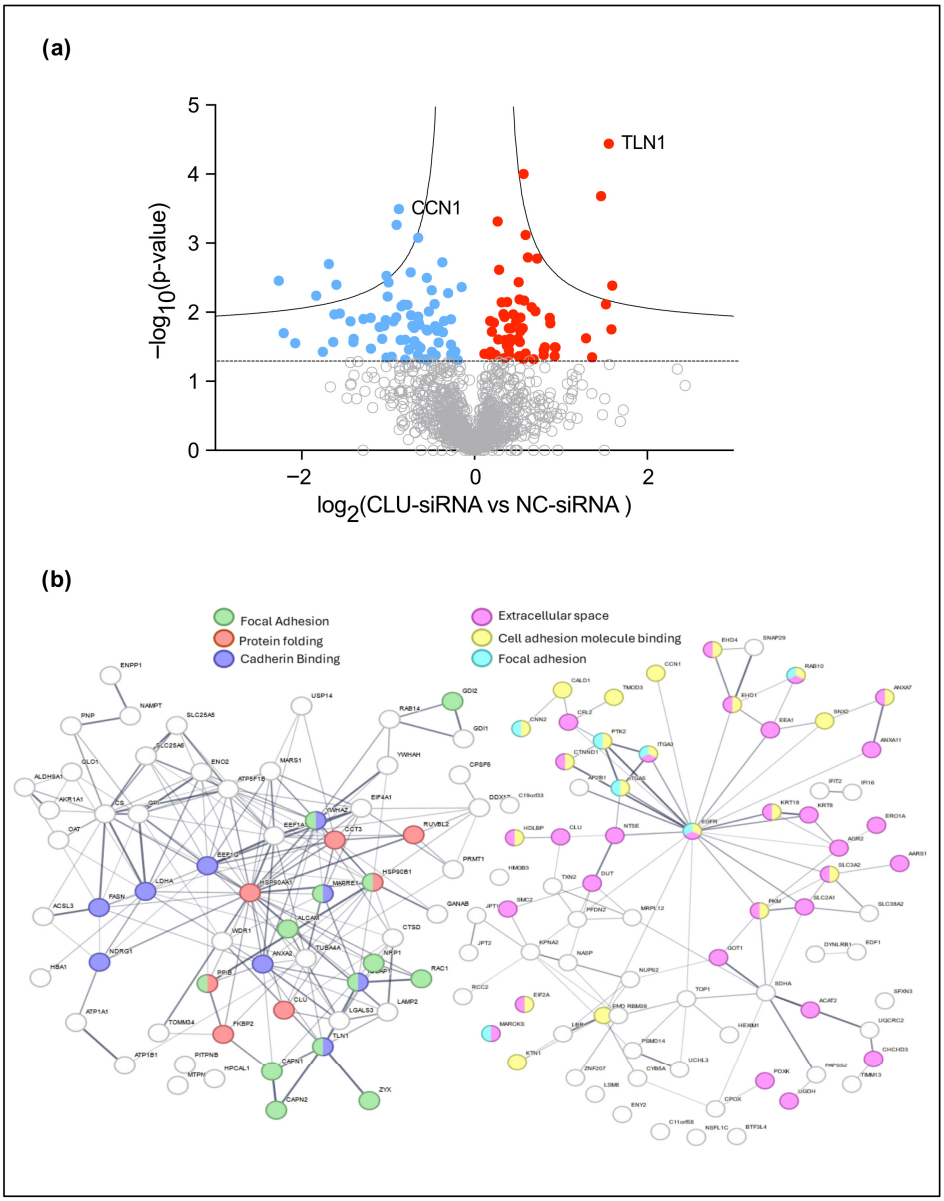



**Figure 7. Proteomic effects of CLU silencing on MDA-MB-231 cells.** Volcano plot showing −log10 of *p*-values versus log2 of the protein ratio between CLU-siRNA and NC-siRNA MDA-MB-231 cells of 1197 proteins (n = 3). The horizontal dashed line indicates –log10(*p*-value) of 1.3, which corresponds to a *p*-value of 0.05. Proteins above this line are considered significantly regulated (red dots for increased proteins, light blue dots for decreased proteins). The two solid lines (hyperbolas) represent the permutation-based False Discovery Rate (FDR) analysis applied to evaluate the more stringent statistical significance of protein regulation in the two conditions (**a**). Protein–Protein Interaction (PPI) networks generated using the STRING database for up- and downregulated proteins in CLU-silenced cells. Stronger interactions are represented by thicker connecting lines. Proteins involved in specific functions are highlighted with distinct colors (**b**).

Functional enrichment analysis of this exploratory protein set revealed overrepresentation of pathways related to integrin-associated signaling, cadherin-mediated adhesion, focal adhesion, and extracellular space organization (Figure 8). Notably, TLN1 and CCN1, both components of focal adhesion-related pathways, were among the most strongly upregulated and downregulated proteins, respectively, and are highlighted in the volcano plot. While these pathway-level findings are exploratory in nature, they are consistent with the cellular and functional alterations observed upon CLU silencing.

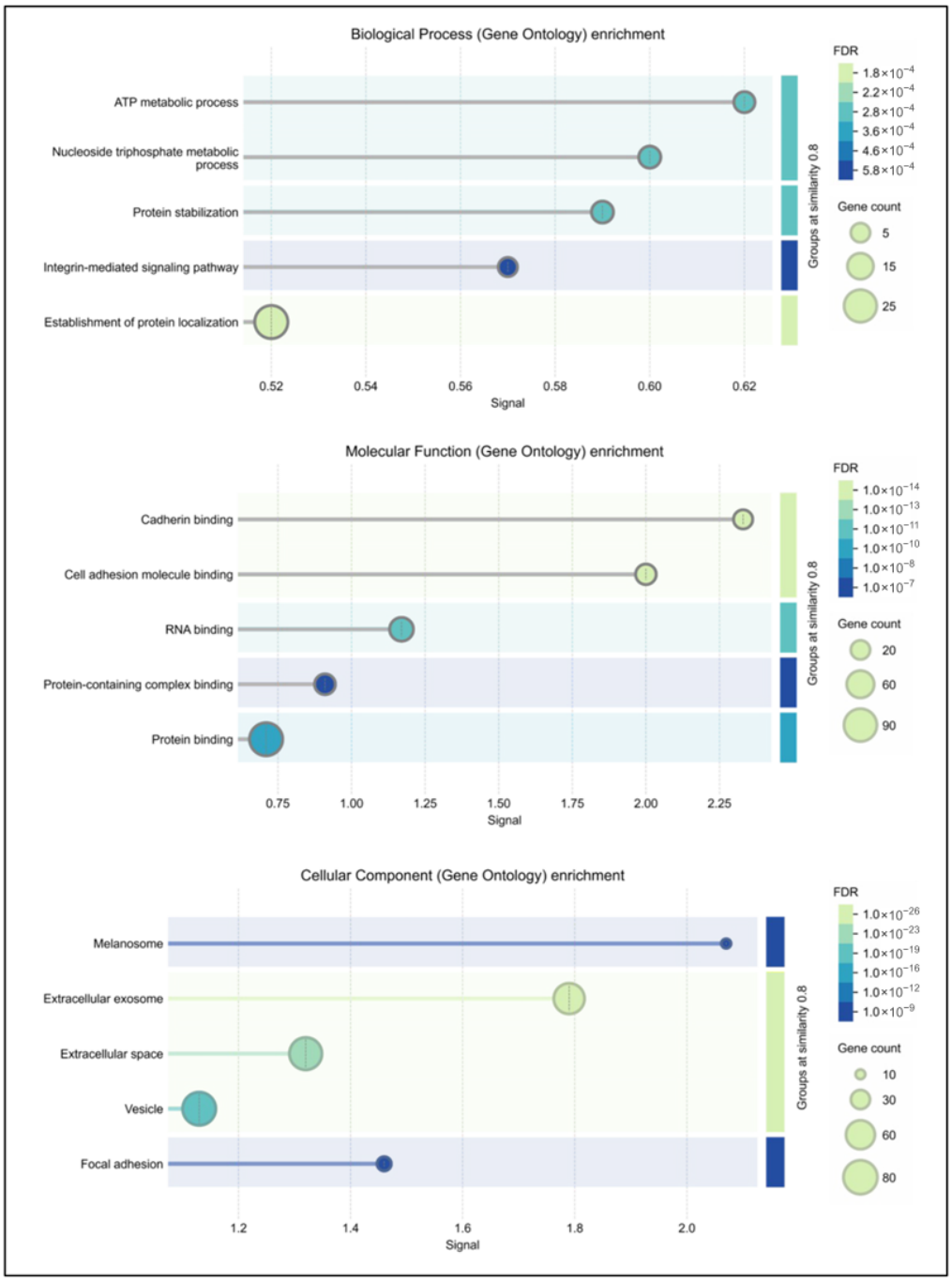



**Figure 8. Functional enrichment analysis of proteins modulated by CLU silencing in MDA-MB-231 cells**. Top 5 enriched Gene Ontology (GO) terms (Biological Process, Molecular Function, Cellular Component) identified through STRING-based functional enrichment analysis.

## 3. Discussion

Metastasis remains the leading cause of breast cancer (BC)-related mortality, accounting for approximately 90% of deaths. During the multi-step metastatic cascade, cancer cells must acquire increased motility and invade the extracellular matrix (ECM) to exit the primary tumor, enter the bloodstream for systemic dissemination, and ultimately home to distant sites [25]. Secreted factors within the tumor microenvironment (TME) critically influence this transition toward an aggressive phenotype.

In this study, we investigated the functional contribution of the secreted glycoprotein clusterin (CLU), whose expression is elevated in malignant breast tissues and further in-

creased in lymph node metastases [17]. Although CLU overexpression is often associated with poor clinical outcomes, whether CLU acts as a true driver of BC aggressiveness or merely reflects tumor progression has remained unresolved. Our work provides mechanistic evidence suggesting that CLU may contribute to metastatic traits, particularly in highly aggressive BC cells.

Using siRNA-mediated depletion of CLU in both invasive MDA-MB-231 and non-invasive MCF-7 cells, we first confirmed effective silencing at both the mRNA and protein levels, with sCLU no longer detectable in the culture medium 48 h after transfection. This time-point was therefore selected for all subsequent assays.

CLU knockdown did not affect the proliferation of either cell line, regardless of the degree of malignancy and differentiation features. Consistently, no significant differences were observed in the activation of the mitogenic kinase ERK. Instead, CLU appeared to regulate, in a cell-specific context, BC cell invasion and migration. In agreement with previous findings [26], sCLU knockdown significantly suppressed motility and invasiveness in MDA-MB-231 cells, a basal-like, triple-negative, highly metastatic subtype [27,28]. Strikingly, this phenotype was absent in MCF-7 cells, which are luminal-like, hormone receptor-positive, and poorly metastatic [27,29]. This context specificity represents a novel finding, suggesting that CLU functions as a pro-migratory factor only in cells already endowed with mesenchymal features.

To explore the underlying mechanisms, we assessed the impact of CLU knockdown on epithelial–mesenchymal transition (EMT). CLU silencing reduced Slug expression in both MCF-7 and MDA-MB-231 cells, whereas Snail expression was selectively upregulated in MCF-7 cells. No detectable changes were observed in E-cadherin or Vimentin levels, which remained restricted to MCF-7 and MDA-MB-231 cells, respectively. These data suggest that CLU may drive a partial reprogramming of EMT-related transcription factors in a cell line-dependent manner without inducing a clear phenotype switch. In addition, it is well known that Slug expression affects other cancer-related processes, such as ECM remodeling and stemness properties acquisition.

Because efficient cell migration requires coordinated remodeling of the actin and microtubule cytoskeleton, we next examined cytoskeletal architecture. In fact, actin polymerization and turnover are required to generate membrane protrusions, while F-actin stress fibers must coordinately work to ensure a dynamic balance of both protrusive and retractile forces supporting cell movement [30,31]. In addition, the regulation of microtubule dynamics is required to coordinate cell polarization, as well as adhesion asymmetry, which is also a requisite for cell movement [22]. Highly motile MDA-MB-231 cells displayed prominent F-actin stress fibers and actin-rich protrusions, consistent with previous reports [32]. CLU knockdown led to loss of membrane protrusions, a reduction in stress fibers, and disorganization of the microtubule network, indicating altered cytoskeletal dynamics and cell polarity. These results suggest that CLU may act as an upstream regulator of the cytoskeletal machinery required for cell motility.

Given the central role of Rho GTPases in cytoskeletal organization [22], we analyzed RhoA activation and found that CLU knockdown markedly reduced GTP-bound RhoA levels without altering total RhoA expression. This observation aligns with prior studies showing that RhoA inhibition suppresses MDA-MB-231 invasiveness [33]. The phosphoinositide 3-kinase (PI3K)/Akt pathway is a vital oncogenic pathway that plays critical roles in multiple aspects of cancer hallmarks, including cell survival, metabolism, metastasis, and angiogenesis [34]. The activation of Akt signaling not only mediates many critical cellular functions but also greatly influences cytoskeletal changes through the regulation of guanine nucleotide exchange factors that promote the activation of the Rho family of small GTPases [24,35]. Of note, CLU silencing in MDA-MB-231 cells induced a reduction

in pAkt, suggesting that CLU may contribute to cytoskeleton remodeling through Akt signaling. We also examined the involvement of the NF-κB pathway, a central regulator of cancer cell survival, inflammation, and metastasis. NF-κB contributes to cancer progression, sustaining a pro-tumorigenic transcriptional program that includes the upregulation of ECM-degrading enzymes [14,36]. In MDA-MB-231 cells, CLU silencing yielded a reduction in NF-kB activity and a concomitant downregulation of MMP9, COL1A1, and COL4A1, further supporting the role of CLU in promoting an invasive phenotype.

The observation that CLU silencing markedly impairs migration, invasion and cytoskeletal dynamics only in MDA-MB-231 cells, while having no significant effects in MCF-7 cells, strongly suggests that CLU's function is context-dependent. In particular, our findings indicate that CLU may promote motility exclusively in cells endowed with a mesenchymal-like, aggressive phenotype and pre-existing EMT traits. This differential response raises the hypothesis that specific membrane receptors or intracellular effectors capable of transducing CLU-mediated signals might be selectively expressed/active in highly invasive BC cells.

Proteomic analysis confirmed that CLU silencing affects multiple proteins involved in cell adhesion, focal adhesion dynamics, cytoskeletal organization, and ECM interactions. TLN1 was identified as the most upregulated protein and CCN1 among the most downregulated following CLU knockdown in MDA-MB-231 cells, reinforcing the hypothesis that CLU modulates focal adhesion dynamics. CCN1 is a matricellular protein that orchestrates cell adhesion and migration through its interaction with various integrins and surface receptors, thereby activating downstream signaling cascades such as FAK, MAPK, and Rho family GTPases [37]. Its expression is transcriptionally regulated by numerous extracellular stimuli, including growth factors, TGF-β1, hypoxia, and inflammatory cytokines, and notably, GPCR-dependent activation of CCN1 transcription has been associated with RhoA-GTP activity [38]. Therefore, the observed reduction in CCN1 upon CLU silencing is consistent with the decrease in RhoA activation we detected through the pull-down assay, suggesting that CLU may act upstream of a RhoA-CCN1 sustaining cytoskeletal remodeling and motility. Of note, in BC, CCN1 protein levels have been positively correlated with tumor size, stage of disease and lymph node involvement, further supporting a pro-migratory and pro-invasive role in BC carcinogenesis [39]. Conversely, TLN1, a multifunctional adaptor protein that links integrins to the actin cytoskeleton, was upregulated in CLU-silenced MDA-MB-231 cells. Beyond its role in integrin activation and focal adhesion assembly, TLN1 also functions as a mechanosensor responsible for the transduction of mechanical forces into biochemical signals between the ECM and the intracellular actomyosin machinery [40]. Of note, its functional output is highly dependent on its conformational state, binding partners, and subcellular localization [40,41]. Therefore, the increased TLN1 expression observed in CLU-silenced cells does not necessarily mean enhanced TLN1 activity. Indeed, TLN1 acts as a force-dependent mechanosensor whose cyclical stretching under mechanical tension, more than its mere expression level, promotes vinculin recruitment and focal adhesion reinforcement [42]. We might speculate that CLU favors the dynamic shift between different structural conformations of TLN1, supporting, in this way, a pro-migratory signaling context. On the contrary, the observed TLN1 upregulation following CLU silencing may correspond to a more stabilized conformation that limits focal adhesion turnover and cytoskeletal plasticity, thereby contributing to the reduced motile phenotype observed.

Altogether, integrating statistically supported proteomic changes with exploratory pathway analyses and functional assays, our data suggest that CLU contributes to the regulation of adhesion stability and cytoskeletal plasticity that underlie cell migration. While further validation will be required to define the precise molecular mechanisms, these

findings identify CLU as a component of the regulatory network controlling breast cancer cell motility and support its potential relevance as a therapeutic target in aggressive breast cancer subtypes.

## 4. Materials and Methods

### 4.1. Cell Culture

Human cell lines MCF7 and MDA-MB-231 were purchased from the American Type Culture Collection (ATCC, Manassas, VA, USA). The cells were cultured in RPMI 1640 (#10-041-CV, Corning® RPMI 1640, Corning, NY, USA) supplemented with 10% Fetal Bovine Serum (FBS) (#A5256701, Thermo Fisher Scientific, Waltham MA, USA) and 100 U/mL penicillin and 100 µg/mL streptomycin (#15140-122, Thermo Fisher Scientific, Waltham MA, USA) and maintained at 37 °C in a humidified atmosphere, supplied with 5% $CO_2$. Cell growth was monitored daily, the culture medium was changed every 2–3 days, and cells were subcultured when they reached 80–90% confluence. Cell harvesting was performed using a Trypsin/Ethylenediaminetetraacetic acid (EDTA) solution (#15400-054, Thermo Fisher Scientific, Waltham, MA, USA). The cultured cells were regularly examined for the presence of mycoplasma contamination using PCR analysis.

### 4.2. siRNA Transfection

Cells were transfected with Clusterin-siRNA (CLU-siRNA, 5′-GCAGCAGAGUCUUCA UCAU-3′, Ambion, Austin, TX, USA) and non-silencing-siRNA (NC-siRNA, Integrated DNA Technologies, Coraville, CA, USA). Briefly, the cells were seeded at a density of $2 \times 10^5$ cells/mL in RPMI 10%. Once the cells were attached, the medium was replaced with 1.75 mL RPMI 1%. Twenty-four hours after seeding, 250 µL of a transfection mix made of Opti-MEM™ medium, Lipofectamine® RNAiMAX Reagent (Thermo Fisher Scientific, Waltham, MA, USA), and 10 nM of CLU-siRNA or NC-siRNA was transferred to the cells and incubated at 37 °C and 5% $CO_2$ for 48 h.

### 4.3. Migration and Invasion Assays

The migratory and invasive capacity of MCF-7 and MDA-MB-231 carrying NC-siRNA or CLU-siRNA was evaluated using 8 µm pore polycarbonate membrane inserts (Corning Transwell®, Corning, NY, USA) placed in a 24-well cell culture plate. A total of $5 \times 10^4$ cells/mL were seeded in the upper compartment in 200 µL of serum-free RPMI, while 600 µL of RPMI 10% FBS was added in the lower compartment as a chemoattractant. To evaluate cell invasion, polycarbonate membrane inserts were coated with basement membrane matrix (300 µg/mL Corning Matrigel® Matrix, Corning, NY, USA) diluted in a coating buffer (0.01 M Tris pH 8, 0.7% NaCl) before cell seeding. After 24 h of incubation at 37 °C, 5% $CO_2$, migrated/invaded cells were fixed using 4% Paraformaldehyde (PFA) in PBS 1× for 5 min at room temperature and then stained with 0.5% crystal violet (Sigma-Aldrich, St. Louis, MO, USA) in 20% methanol for 15 min. Fixed and stained cells were counted under an optical microscope, selecting three different fields for each observed insert. For rescue experiments, 2 µg/mL of recombinant human CLU protein (BioLegend, San Diego, CA, USA) was added at the time of seeding and maintained for the entire duration (24 h) of the transwell migration assay in CLU-silenced MDA-MB-231 cells. Each experimental condition was analyzed in triplicate inserts (technical replicates), and the entire experiment was independently repeated three times (biological replicates).

### 4.4. Cell Viability Assay

Cell viability was evaluated through the ATPlite Luminescence Assay (PerkinElmer, Waltham, MA, USA), an ATP monitoring system based on luciferase activity. A total of

$5 \times 10^4$ cells/mL were seeded in a 96-well plate following siRNA transfection. Then, 50 µL of lysis buffer, followed by 50 µL of the substrate, was added to each well of the plate on a shaker for 5 min. The plate was then incubated and protected from light for 10 min. Luminescence was measured using the EnSpire® Multimode Plate Reader (PerkinElmer, Waltham, MA, USA) instrument. Each experimental condition was analyzed in four technical replicates, and the entire experiment was independently repeated three times (biological replicates).

### 4.5. RNA Extraction and cDNA Synthesis

Cells were washed in PBS 1× (100 mL of PBS 10× in 900 mL of $H_2O$) and lysed using 1 mL of TRIzol Reagent (#15596026, ThermoFisher Scientific, Waltham, MA, USA). After adding 200 µL of chloroform, the cells were shaken and centrifuged at 14,000 rpm for 30 min at 4 °C. The upper aqueous phase containing the RNA was taken and mixed with an equal volume of ethanol 95–100%. RNA extraction and purification were performed using an RNA Clean & Concentrator™-5 kit (Zymo Research, Irvine, CA, USA) according to the manufacturer's instructions. RNA was eluted with 15 µL of DNase/RNase-Free Water and quantified using a NanoPhotometer® N50 (Implen, Munich, Germany). A total of 500 ng of RNA was reverse transcribed using a RevertAid First Strand cDNA Synthesis Kit (ThermoFisher Scientific™, Waltham, MA, USA) with 1 µL of Random Primers following the manufacturer's instructions. cDNA was stored at −20 °C or used for qRT-PCR analysis as described below.

### 4.6. qRT-PCR Analysis

Table 1 shows the primer sequences used for qRT-PCR analyses. A total of 1 µL of each cDNA sample was mixed with 0.5 µL of 10µM Forward Primer and Reverse Primer, 10 µL of SsoAdvancedTM Universal SYBR® Green Supermix (Bio-Rad, Berkley, CA, USA), and 8 µL of DNase-free water. The expression of each gene was normalized to Glyceraldehyde 3-phosphate dehydrogenase (GAPDH). All reactions were performed twice using the MJ Opticon 4 (MJ Research, Waltham, MA, USA) system. The thermocycling included an initial step at 95 °C (30 s), followed by 40 amplification cycles: denaturation at 95 °C (5 s) and annealing/extension at 60 °C (30 s). The fold-change of gene expression was determined using the comparative $2^{-\Delta\Delta CT}$ method.

**Table 1.** Primer sequences used for qRT-PCR.

| | Forward 5′-3′ | Reverse 5′-3′ |
|---|---|---|
| CLU | TGATCCCATCACTGTGACGG | GCTTTTTGCGGTATTCCTGC |
| Snail | CCCCAATCGGAAGCCTAACT | GACAGAGTCCCAGATGAGCA |
| Slug | TGCATATTCGGACCCACACA | GGTCTGCAGATGAGCCCTC |
| MMP2 | ACTGTGACGCCACGTGAACCAA | CGTATACCGCATCAATCTTTCC |
| MMP9 | GGCCCTTCTACGGCCACT | CAGAGAATCGCCAGTACTT |
| COL1a1 | TCGGAGGAGAGTCAGGAAGG | TCAGCAACACAGTTACACAAGGA |
| COL4a1 | CAAAAGGGTGATACTGGAGAACC | ATTTCCAGCGAAACCAGGCA |
| GAPDH | AACCTGCCAAATATGATGAC | TTGAAGTCAGAGGAGACCAC |

### 4.7. Protein Extraction and Quantification

Cells were washed twice in PBS 1× and harvested in 100 µL of RIPA buffer (50 mM Tris-HCl pH 7.4, 100 mM NaCl, 1% Triton X-100) containing 1% of protease and phosphatase inhibitor cocktails (Sigma-Aldrich, St. Louis, MO, USA). The cells were maintained on a shaker at 4 °C for 1 h and centrifuged at 12,000 rpm at 4 °C for 30 min. After collecting the supernatant, total proteins were quantified with the Lowry method using a Bio-Rad DC Protein assay (Bio-Rad, Hercules, CA, USA). Briefly, 5 µL of samples or Bovine Serum

Albumin (BSA) (Sigma-Aldrich, St. Louis, MO, USA) standards were incubated with 25 µL of Reagent A' (20 µL of Reagent S in 1 mL of Reagent A) and 200 µL of Reagent B for 15 min protected from light. Absorbance was read at 750 nm through an EnSpire® Multimode Plate Reader (PerkinElmer, Waltham, MA, USA) spectrophotometer.

### 4.8. Active Rho Pull-Down Assay

Intracellular levels of active GTP-bound RhoA were assessed using an Active Rho Pull-Down and Detection Kit (ThermoFisher, cat. n. 16116) according to the manufacturer's instructions. Briefly, 100 µL of the 50% resin slurry was added to the spin cups with collection tubes and centrifuged at 6000× *g* for 30 s. Then, 400 µL of Lysis/Binding/Wash Buffer was added to each tube with resin and centrifuged at 6000× *g* for 30 s. Then, 400 µg of GST-Rhotekin-RBD and 500 µg of total proteins were incubated at 4 °C for 1 h and centrifuged at 6000× *g* for 30 s. Resins were washed three times and resuspended with 50 µL of reducing buffer (1 part of β-mercaptoethanol to 20 parts of 2X SDS Sample Buffer). After resin removal by centrifugation, the eluted samples were heated for 5 min at 95–100 °C; 25 µL/sample was used for SDS-PAGE and Western blotting. Membranes were probed with Anti-Rho Antibody and then with horseradish peroxidase-conjugated secondary antibody provided with the kit. To ensure the pull-down reactions were working properly, a positive control with GTPγS treatment was performed.

### 4.9. SDS-PAGE and Western Blot

Total proteins were separated using 12% Polyacrylamide Tris-Glycine gels under reducing conditions and transferred to 0.45 µm polyvinylidene difluoride (PVDF) membranes (#IPVH00010, Merck Millipore, Darmstadt, Germany). Molecular weight estimation was performed using a PageRuler Plus Prestained Protein Ladder (#26619, ThermoFisher Scientific, Waltham, MA, USA). Protein blotting was performed in Tris-Glycine buffer (Tris 48 mM, Glycine 39 mM, 10% methanol in deionized $H_2O$) for 1 h at 90 V at 4 °C. Transfer efficiency was verified with Red Ponceau S (Sigma-Aldrich, St. Louis, MO, USA). Membranes were blocked with a TTBS 1× solution (50 mM Tris-HCl, pH 7.5, 150 mM NaCl, 0.1% Tween 2.0) containing 5% nonfat dried milk or 3% BSA, depending on the primary antibody used. The membranes were sequentially incubated in primary antibodies (Table 2) and then with appropriate horseradish peroxidase-conjugated secondary antibodies (Table 3). Signals were visualized using BM Chemiluminescence Blotting Substrate (POD) (Roche Diagnostics GmbH, Mannheim, Germany) and Blue Devil Autoradiography films (Genesee Scientific, El Cajon, CA, USA). Densitometric quantification of the bands was performed with ImageJ software (version 1.54g) (National Institute of Health, Bethesda, MD, USA), normalizing the values of all samples to the value measured for the β-actin band.

**Table 2.** Primary antibodies used for Western blot and immunocytochemistry.

| Antibody | Species | Method/Dilution |
|---|---|---|
| Anti-CLU (AF2937, R&D System, Minneapolis, MN, USA) | Goat | WB 1:1000 |
| Anti-Akt (9272, Cell Signaling, Danvers, MA, USA) | Rabbit | WB 1:1000 |
| Anti-pAkt (9271, Cell Signaling) | Rabbit | WB 1:500 |
| Anti-NF-kB (6956, Cell Signaling) | Mouse | WB 1:1000 |
| Anti-pNF-kB p65 (3033, Cell Signaling) | Rabbit | WB 1:200 |
| Anti-ERK (9102, Cell Signaling) | Rabbit | WB 1:1000 |
| Anti-pERK (9101, Cell Signaling) | Rabbit | WB 1:1000 |
| Anti-E-cadherin (610182, BD, Franklin Lakes, NJ, USA) | Mouse | WB 1:1000<br>ICC 1:50 |
| Anti-Vimentin (5741, Cell Signaling) | Rabbit | WB 1:1000<br>ICC 1: 200 |
| Anti-α-tubilin (T6199, Sigma-Aldrich) | Mouse | ICC 1:200 |
| Anti-β-actin (GXGTX109639, GeneTex, Irvine, CA, USA) | Rabbit | WB 1:500 |

WB = Western blot; ICC = immunocytochemistry.

**Table 3.** Secondary antibodies used for Western blot and immunocytochemistry.

| Antibody | Species | Method/Dilution |
|---|---|---|
| Anti-Mouse IgG-Peroxidase antibody (A5906, Sigma-Aldrich, St. Louis, MO, USA) | Sheep | WB 1:5000 |
| Anti-Goat IgG-Peroxidase antibody (A8919, Sigma-Aldrich) | Rabbit | WB 1:5000 |
| Anti-Rabbit IgG-Peroxidase antibody (A0545, Sigma-Aldrich) | Goat | WB 1:80,000 |
| Anti-Mouse IgG (Alexa FlourTM 568, Invitrogen) | Goat | ICC 1:500 |
| Anti-Rabbit IgG (Alexa FlourTM 488, Invitrogen) | Goat | ICC 1:300 |
| Anti-Mouse IgG (Alexa FlourTM 488, Invitrogen) | Goat | ICC 1:500 |
| Anti-Rabbit IgG-Peroxidase antibody (ThermoFisher) | Goat | WB 1:500 |

WB = Western blot; ICC = immunocytochemistry.

### 4.10. Immunocytochemistry and Confocal Microscopy

Cells were seeded on glass coverslips at $5 \times 10^4$ cells/mL density, maintained at 37 °C and 5% $CO_2$ for 24 h, and transfected with CLU-siRNA or NC-siRNA. After 48 h, cells were washed in PBS 1×, fixed with 4% PFA in PBS 1×, permeabilized with PBS 1×-0.25% Triton X-100, and blocked with 5% BSA. Glass coverslips were sequentially incubated with primary antibodies (Table 2) and then with appropriate fluorescent secondary antibodies (Table 3). F-actin staining was performed with Alexa Fluor 633 phalloidin. Nuclei were stained with 4′,6-diamidino-2-phenylindole (DAPI) (Sigma-Aldrich, St. Louis, MO, USA). Glass coverslips were mounted with Mowiol (Sigma-Aldrich, St. Louis, MO, USA). Confocal images were acquired using a Leica STELLARIS system equipped with a White Light Laser (WLL) and a 405 nm diode laser, integrated with high-sensitivity HyD spectral detectors and an inverted DMi8 microscope. All images were captured using an HC PL APO CS2 40x/1.30 NA oil immersion objective. Phalloidin 633, Alexa 568 and Alexa 488 were excited with the 633 nm, 561 nm and 490 nm lines of the WLL, respectively, with spectral emission collected in the range 650–690 nm for phalloidin, 600–640 for Alexa 568 and 530–570 nm for Alexa 488. DAPI was excited using the 405 nm diode laser line, and emission was collected between 470 and 500 nm. Image acquisition was managed through Leica Las X software and performed in sequential mode with a pinhole aperture set at 1.0 Airy unit.

### 4.11. Proteomic Analysis

After transfection, cells were washed twice in PBS 1× and collected in STET buffer (50 mM Tris, pH 7,5, 150 mM NaCl, 2 mM EDTA, 1% Triton), supplemented with protease inhibitor cocktail. A total of 50 µg of extracted protein was digested using an iST 96X kit (PreOmics, Planegg, Germany), according to the manufacturer's instructions. Briefly, samples were denatured at 95 °C for 10 min and then loaded into the supplied cartridge. Digestion was carried out at 37 °C for 3 h. The resulting peptides were eluted, vacuum-dried and resuspended in LC-load provided by the kit.

Peptides were separated using a Vanquish Neo nanoUHPLC system coupled online to an Orbitrap Exploris 480 mass spectrometer, equipped with a 75 µm × 25 cm Acclaim PepMap RSLC analytical column (instruments and columns from Thermo Fisher Scientific). Peptide separation was achieved using a 110 min binary gradient of acetonitrile in water (0–100%), both containing 0.1% formic acid. Data-independent acquisition (DIA) was used for label-free quantification of peptides. DIA was performed using an MS1 full scan (380 $m/z$ to 980 $m/z$) followed by 49 sequential DIA windows with a 12 $m/z$ with 1 $m/z$ of overlap. Full scans were acquired at a resolution of 120.000, with an automatic gain control (AGC) of 3 × 106, and a maximum injection time of 50 ms. Afterwards, 49 isolation windows were scanned at 30.000 resolution, with an AGC of 8 × 105 and the maximum injection time set to "auto". The scan range ($m/z$) was set at 145–1450, and the HCD collision energy was set at 28%. Data analysis was performed using DIA-NN software (version 2.0.2) on both datasets with a predicted library generated from an in

silico-digested human UniProt reference database (UP000005640_9606), downloaded on 03.04.2025. Digestion allowed cleavage at K and R, with up to two missed cleavages and a minimum peptide length of six. This library consisted of 20,397 protein isoforms, 32,710 protein groups, and 5,495,479 precursors in 2,932,475 elution groups. The FDR for peptide and protein identification was set at 0.01%. Protein quantification was performed using label-free quantification (LFQ). Data analysis and statistical evaluation of changes in protein abundance were conducted in Perseus (version 2.0.9.0).

### *4.12. Statistical Analysis*

The data were analyzed using GraphPad Prism 10 software (Version 10.6.1). Group comparisons were performed using Student's *t*-test, and a $p$-value < 0.05 was considered significant.

## 5. Conclusions

We show that CLU knockdown markedly reduces migration and invasion in highly aggressive BC cells. This phenotype is coupled to pronounced morphological alterations and reduced activation of Akt, NF-κB, and RhoA, as well as decreased MMP9, COL1A1, and COL4A1 expression. Proteomic profiling reveals broad remodeling of adhesion and cytoskeletal networks, including downregulation of CCN1 and upregulation of TLN1, supporting a model in which CLU regulates adhesion–cytoskeleton signaling, with potential downstream effects on mechanotransduction pathways.

This is, to our knowledge, the first study to demonstrate that CLU's role in BC cell motility is strongly context-dependent, being preferentially active in EMT-engaged, basal-like BC cells. Our findings provide a solid rationale for translational studies aimed at evaluating CLU as a therapeutic target in precision oncology settings, particularly for aggressive BC subtypes where metastasis remains a critical unmet challenge.

**Supplementary Materials:** The following supporting information can be downloaded at: https://www.mdpi.com/article/10.3390/ijms27041721/s1.

**Author Contributions:** Conceptualization: F.R.; methodology: A.C. and M.M.; formal analysis: A.C.; investigation: A.C., M.M., S.B., S.D.S., M.L.P. and P.C.; writing (original draft): A.C., F.R. and P.C.; writing (review and editing): A.C. and F.R.; supervision: F.R.; funding acquisition: F.R. All authors have read and agreed to the published version of the manuscript.

**Funding:** This research was funded by MUR PRIN 2017 Grant No. 2017T8CMCY to Federica Rizzi.

**Institutional Review Board Statement:** Not applicable.

**Informed Consent Statement:** Not applicable.

**Data Availability Statement:** Requests to access the datasets should be directed to federica.rizzi@unipr.it (corresponding author).

**Conflicts of Interest:** The authors declare no conflicts of interest.

## Abbreviations

The following abbreviations are used in this manuscript:

| | |
|---|---|
| BC | Breast Cancer |
| ER | Estrogen Receptor |
| PR | Progesterone Receptor |
| HER2 | Human Epidermal Growth Factor Receptor 2 |
| TNBC | Triple-Negative Breast Cancer |
| CLU | Clusterin |
| sCLU | Secreted Clusterin |
| EMT | Epithelial–Mesenchymal Transition |

| | |
|---|---|
| ECM | Extracellular Matrix |
| ATCC | American Type Culture Collection |
| FBS | Fetal Bovine Serum |
| EDTA | Ethylenediaminetetraacetic acid |
| PFA | Paraformaldehyde |
| BSA | Bovine Serum Albumin |
| PVDF | Polyvinylidene difluoride |
| DAPI | 4′,6-diamidino-2-phenylindole |
| WB | Western Blot |
| ICC | Immunocytochemistry |
| CLSM | Confocal Laser Scanning Microscopy |
| MMPs | Metalloproteases |
| PI3K | Phosphoinositide 3-kinase |
| TLN1 | Talin-1 |
| CCN1 | CCN family member 1 |

## References


1. Bray, F.; Laversanne, M.; Sung, H.; Ferlay, J.; Siegel, R.L.; Soerjomataram, I.; Jemal, A. Global cancer statistics 2022: GLOBOCAN estimates of incidence and mortality worldwide for 36 cancers in 185 countries. *CA Cancer J. Clin.* **2024**, *74*, 229–263. [CrossRef]
2. Maisonneuve, P.; Disalvatore, D.; Rotmensz, N.; Curigliano, G.; Colleoni, M.; Dellapasqua, S.; Pruneri, G.; Mastropasqua, M.G.; Luini, A.; Bassi, F.; et al. Proposed new clinicopathological surrogate definitions of luminal A and luminal B (HER2-negative) intrinsic breast cancer subtypes. *Breast Cancer Res.* **2014**, *16*, R65. [CrossRef]
3. Łukasiewicz, S.; Czeczelewski, M.; Forma, A.; Baj, J.; Sitarz, R.; Stanisławek, A. Breast cancer-epidemiology, risk factors, classification, prognostic markers, and current treatment strategies-an updated review. *Cancers* **2021**, *13*, 4287. [CrossRef]
4. Prat, A.; Pineda, E.; Adamo, B.; Galván, P.; Fernández, A.; Gaba, L.; Díez, M.; Viladot, M.; Arance, A.; Muñoz, M. Clinical implications of the intrinsic molecular subtypes of breast cancer. *Breast* **2015**, *24*, S26–S35. [CrossRef]
5. Blaschuk, O.; Burdzy, K.; Fritz, I.B. Purification and characterization of a cell-aggregating factor (clusterin), the major glycoprotein in ram rete testis fluid. *J. Biol. Chem.* **1983**, *258*, 7714–7720. [CrossRef]
6. Wilson, M.R.; Zoubeidi, A. Clusterin as a therapeutic target. *Expert Opin. Ther. Targets* **2017**, *21*, 201–213. [CrossRef]
7. Bonacini, M.; Coletta, M.; Ramazzina, I.; Naponelli, V.; Modernelli, A.; Davalli, P.; Bettuzzi, S.; Rizzi, F. Distinct promoters, subjected to epigenetic regulation, drive the expression of two clusterin mRNAs in prostate cancer cells. *Biochim. Biophys. Acta* **2015**, *1849*, 44–54. [CrossRef]
8. Rodríguez-Rivera, C.; Garcia, M.M.; Molina-Álvarez, M.; González-Martín, C.; Goicoechea, C. Clusterin: Always protecting. Synthesis, function and potential issues. *Biomed. Pharmacother.* **2021**, *134*, 111174. [CrossRef] [PubMed]
9. Panico, F.; Casali, C.; Rossi, G.; Rizzi, F.; Morandi, U.; Bettuzzi, S.; Davalli, P.; Corbetta, L.; Storelli, E.S.; Corti, A.; et al. Prognostic role of clusterin in resected adenocarcinomas of the lung. *Lung Cancer* **2013**, *79*, 294–299. [CrossRef]
10. Rizzi, F.; Bettuzzi, S. Clusterin (CLU) and prostate cancer. *Adv. Cancer Res.* **2009**, *105*, 1–19. [CrossRef] [PubMed]
11. Trougakos, I.P. The molecular chaperone apolipoprotein J/clusterin as a sensor of oxidative stress: Implications in therapeutic approaches—A mini-review. *Gerontology* **2013**, *59*, 514–523. [CrossRef]
12. Zhang, Y.; Lv, X.; Chen, L.; Liu, Y. The role and function of CLU in cancer biology and therapy. *Clin. Exp. Med.* **2023**, *23*, 1375–1391. [CrossRef]
13. Rizzi, F.; Bettuzzi, S. The clusterin paradigm in prostate and breast carcinogenesis. *Endocr. Relat. Cancer* **2010**, *17*, R1–R17. [CrossRef] [PubMed]
14. Bonacini, M.; Negri, A.; Davalli, P.; Naponelli, V.; Ramazzina, I.; Lenzi, C.; Bettuzzi, S.; Rizzi, F. Clusterin Silencing in Prostate Cancer Induces Matrix Metalloproteinases by an NF-κB-Dependent Mechanism. *J. Oncol.* **2019**, *2019*, 4081624. [CrossRef] [PubMed]
15. Bettuzzi, S.; Davalli, P.; Davoli, S.; Chayka, O.; Rizzi, F.; Belloni, L.; Pellacani, D.; Fregni, G.; Astancolle, S.; Fassan, M.; et al. Genetic inactivation of ApoJ/clusterin: Effects on prostate tumourigenesis and metastatic spread. *Oncogene* **2009**, *28*, 4344–4352. [CrossRef] [PubMed]
16. Redondo, M.; Téllez, T.; Roldan, M.J.; Serrano, A.; García-Aranda, M.; Gleave, M.E.; Hortas, M.L.; Morell, M. Anticlusterin treatment of breast cancer cells increases the sensitivities of chemotherapy and tamoxifen and counteracts the inhibitory action of dexamethasone on chemotherapy-induced cytotoxicity. *Breast Cancer Res.* **2007**, *9*, R86. [CrossRef]
17. Redondo, M.; Villar, E.; Torres-Muñoz, J.; Tellez, T.; Morell, M.; Petito, C.K. Overexpression of clusterin in human breast carcinoma. *Am. J. Pathol.* **2000**, *157*, 393–399. [CrossRef]

18. Wang, Y.; Brodsky, A.S.; Xiong, J.; Lopresti, M.L.; Yang, D.; Resnick, M.B. Stromal clusterin expression predicts therapeutic response to neoadjuvant chemotherapy in triple negative breast cancer. *Clin. Breast Cancer* **2018**, *18*, e373–e379. [CrossRef]
19. So, A.; Sinnemann, S.; Huntsman, D.; Fazli, L.; Gleave, M. Knockdown of the cytoprotective chaperone, clusterin, chemosensitizes human breast cancer cells both in vitro and in vivo. *Mol. Cancer Ther.* **2005**, *4*, 1837–1849. [CrossRef]
20. Chia, S.; Dent, S.; Ellard, S.; Ellis, P.M.; Vandenberg, T.; Gelmon, K.; Powers, J.; Walsh, W.; Seymour, L.; Eisenhauer, E.A. Phase II trial of OGX-011 in combination with docetaxel in metastatic breast cancer. *Clin. Cancer Res.* **2009**, *15*, 708–713. [CrossRef]
21. Brabletz, S.; Schuhwerk, H.; Brabletz, T.; Stemmler, M.P. Dynamic EMT: A multi-tool for tumor progression. *EMBO J.* **2021**, *40*, e108647. [CrossRef]
22. Dogterom, M.; Koenderink, G.H. Actin-microtubule crosstalk in cell biology. *Nat. Rev. Mol. Cell Biol.* **2019**, *20*, 38–54. [CrossRef]
23. Fife, C.M.; McCarroll, J.A.; Kavallaris, M. Movers and shakers: Cell cytoskeleton in cancer metastasis: Cytoskeleton and cancer metastasis. *Br. J. Pharmacol.* **2014**, *171*, 5507–5523; Erratum in *Br. J. Pharmacol.* **2017**, *174*, 116. [CrossRef]
24. Spiering, D.; Hodgson, L. Dynamics of the Rho-family small GTPases in actin regulation and motility. *Cell Adh Migr.* **2011**, *5*, 170–180. [CrossRef]
25. Fares, J.; Fares, M.Y.; Khachfe, H.H.; Salhab, H.A.; Fares, Y. Molecular principles of metastasis: A hallmark of cancer revisited. *Signal Transduct. Target. Ther.* **2020**, *5*, 28. [CrossRef] [PubMed]
26. Niu, Z.; Li, X.; Hu, B.; Li, R.; Wang, L.; Wu, L.; Wang, X. Small interfering RNA targeted to secretory clusterin blocks tumor growth, motility, and invasion in breast cancer. *Acta Biochim. Biophys. Sin.* **2012**, *44*, 991–998. [CrossRef] [PubMed]
27. Dai, X.; Cheng, H.; Bai, Z.; Li, J. Breast cancer cell line classification and its relevance with breast tumor subtyping. *J. Cancer* **2017**, *8*, 3131–3141. [CrossRef]
28. Ciringione, A.; Rizzi, F. Facing the Challenge to Mimic Breast Cancer Heterogeneity: Established and Emerging Experimental Preclinical Models Integrated with Omics Technologies. *Int. J. Mol. Sci.* **2025**, *26*, 4572. [CrossRef] [PubMed]
29. Ziegler, E.; Hansen, M.-T.; Haase, M.; Emons, G.; Gründker, C. Generation of MCF-7 cells with aggressive metastatic potential in vitro and in vivo. *Breast Cancer Res. Treat.* **2014**, *148*, 269–277; Erratum in *Breast Cancer Res. Treat.* **2016**, *156*, 209–210. [CrossRef]
30. Aseervatham, J. Cytoskeletal remodeling in cancer. *Biology* **2020**, *9*, 385. [CrossRef]
31. Schaks, M.; Giannone, G.; Rottner, K. Actin dynamics in cell migration. *Essays Biochem.* **2019**, *63*, 483–495. [CrossRef]
32. Yamamoto, Y.; Hayashi, Y.; Sakaki, H.; Murakami, I. Downregulation of fascin induces collective cell migration in triple negative breast cancer. *Oncol. Rep.* **2023**, *50*, 150. [CrossRef] [PubMed]
33. Pillé, J.-Y.; Denoyelle, C.; Varet, J.; Bertrand, J.-R.; Soria, J.; Opolon, P.; Lu, H.; Pritchard, L.L.; Vannier, J.P.; Malvy, C.; et al. Anti-RhoA and anti-RhoC siRNAs inhibit the proliferation and invasiveness of MDA-MB-231 breast cancer cells in vitro and in vivo. *Mol. Ther.* **2005**, *11*, 267–274. [CrossRef]
34. Hennessy, B.T.; Smith, D.L.; Ram, P.T.; Lu, Y.; Mills, G.B. Exploiting the PI3K/AKT pathway for cancer drug discovery. *Nat. Rev. Drug Discov.* **2005**, *4*, 988–1004. [CrossRef]
35. McCormick, B.; Chu, J.Y.; Vermeren, S. Cross-talk between Rho GTPases and PI3K in the neutrophil. *Small GTPases* **2019**, *10*, 187–195. [CrossRef] [PubMed]
36. Takeda, T.; Tsubaki, M.; Genno, S.; Tomita, K.; Nishida, S. RANK/RANKL axis promotes migration, invasion, and metastasis of osteosarcoma via activating NF-κB pathway. *Exp. Cell Res.* **2024**, *436*, 113978. [CrossRef]
37. Kerek, R.; Awad, J.S.; Bassam, M.; Hajjar, C.; Ghantous, F.; Rizk, K.; Rima, M. The multifunctional protein CCN1/CYR61: Bridging physiology and disease. *Exp. Mol. Pathol.* **2025**, *142*, 104969. [CrossRef]
38. Walsh, C.T.; Stupack, D.; Brown, J.H. G Protein-Coupled Receptors Go Extracellular: RhoA Integrates the Integrins. *Mol. Interv.* **2008**, *8*, 165–173. [CrossRef]
39. O'Kelly, J.; Chung, A.; Lemp, N.; Chumakova, K.; Yin, D.; Wang, H.J.; Said, J.; Gui, D.; Miller, C.W.; Karlan, B.Y.; et al. Functional domains of CCN1 (Cyr61) regulate breast cancer progression. *Int. J. Oncol.* **2008**, *33*, 59–67. [CrossRef]
40. Zhao, Y.; Lykov, N.; Tzeng, C. Talin-1 interaction network in cellular mechanotransduction (Review). *Int. J. Mol. Med.* **2022**, *49*, 60. [CrossRef]
41. Goult, B.T.; Yan, J.; Schwartz, M.A. Talin as a mechanosensitive signaling hub. *J. Cell Biol.* **2018**, *217*, 3776–3784. [CrossRef] [PubMed]
42. Klapholz, B.; Brown, N.H. Talin—The master of integrin adhesions. *J. Cell Sci.* **2017**, *130*, 2435–2446. [CrossRef] [PubMed]


**Disclaimer/Publisher's Note:** The statements, opinions and data contained in all publications are solely those of the individual author(s) and contributor(s) and not of MDPI and/or the editor(s). MDPI and/or the editor(s) disclaim responsibility for any injury to people or property resulting from any ideas, methods, instructions or products referred to in the content.